Anthropogenic carbon release rate unprecedented during past 66 million years

Richard E. Zeebe[1,*], Andy Ridgwell[2,3], and James C. Zachos[4]

[*]Corresponding Author.

[1]School of Ocean and Earth Science and Technology, University of Hawaii at Manoa, 1000 Pope Road, MSB 629, Honolulu, HI 96822, USA. zeebe@soest.hawaii.edu

[2]School of Geographical Sciences, University of Bristol, UK. andy@seao2.org

[3]Department of Earth Sciences, University of California, Riverside, USA.

[4]Earth and Planetary Sciences Department, University of California, Santa Cruz, USA. jzachos@ucsc.edu

January 31, 2016

Revised Version

Nature Geoscience

Carbon release rates from anthropogenic sources reached a record high of $\sim$10 Pg C yr^{-1} in 2014. Geologic analogues from past transient climate changes could provide invaluable constraints on the response of the climate system to such perturbations, but only if the associated carbon release rates can be reliably reconstructed. The Paleocene-Eocene Thermal Maximum (PETM) is currently known to have the highest carbon release rates of the past 66 million years, but robust estimates of the initial rate and onset duration are hindered by uncertainties in age models. Here we introduce a method to extract rates of change from a sedimentary record based on the relative timing of climate and carbon cycle changes, without the need for an age model. We apply this method to stable carbon and oxygen isotope records from the New Jersey Shelf using time-series analysis and carbon cycle–climate modeling. We calculate that the initial carbon release during the onset of the PETM occurred over at least 4,000 years. This constrains the maximum sustained PETM carbon release rate to less than 1.1 Pg C yr^{-1}. We conclude that, given currently available records, the present anthropogenic carbon release rate is unprecedented during the past 66 million years. We suggest that such a 'no-analogue' state represents a fundamental challenge in constraining future climate projections. Also, future ecosystem disruptions will likely exceed the relatively limited extinctions observed at the PETM.

As rapid reductions in anthropogenic carbon emissions[1] appear increasingly unlikely in the near future, forecasting the Earth system's response to ever-increasing emission rates has become a high priority focus of climate research. Because climate model simulations and projections have large uncertainties – often due to the uncertain strength of feedbacks[2] – geologic analogues from past climate events are invaluable in understanding the impacts of massive carbon release on the Earth system[3,4]. The fastest known, massive carbon release throughout the Cenozoic (past 66 Myr) occurred at the onset of the Paleocene-Eocene Thermal Maximum ($\sim$56 Myr ago)[5–9]. The PETM was associated with a $\sim$5 K surface temperature warming and an estimated total carbon release somewhere between current assessments of fossil fuel reserves (1000$-$2000 Pg C) and resources ($\sim$3,000$-$13,500 Pg C)[10,11]. While the PETM is widely considered the best analogue for present/future carbon release, the time scale of its onset and hence the initial carbon release rate have hitherto remained largely unconstrained. Determining the release rate is critical, however, if we are to draw future inferences from observed climate, ecosystem, and ocean chemistry changes during the PETM[3,7,8,12,13]. If anthropogenic emissions rates have no analogue in Earth's recent history, then unforeseeable future responses of the climate system are possible.

Extracting rates without an age model

Carbon and oxygen isotope records ($\delta^{13}C$, $\delta^{18}O$) of the PETM exist for various marine sections spanning pelagic to shallow marine depositional environments. Pelagic records have robust stratigraphic control, but given relatively slow sedimentation rates and carbonate dissolution, lack the fidelity required to assess the rate of the carbon isotope excursion (CIE) onset[14,15]. The most expanded marine records are found in shelf siliciclastic settings where sedimentation rates are as much as 10$\times$ higher and the effects of carbonate dissolution are minimal[16]. Despite the lack of accurate stratigraphic age control, these records have the greatest potential to resolve the relative phasing between carbon cycle and climate changes.

Our advance here is to recognize that an age model is not strictly necessary in order to extract rates of change from the geological record. Critically, while $\delta^{13}C$ tracks the timing of the carbon release, $\delta^{18}O$ tracks the climate response to CO_2 and other forcings. The climate response is not instantaneous but shows a characteristic temporal delay depending on the climate system's thermal inertia[17–19]. For instance, the rate at which Earth's surface temperature approaches a new equilibrium critically depends on the ocean's heat uptake efficiency. While the initial few % of the response may be achieved within decades, the final few % can take up to millennia. Thus, the absence of a detectable lag between $\delta^{13}C$ and $\delta^{18}O$ in any high fidelity record spanning the PETM onset requires that the onset occurred slower than some threshold. Otherwise, if say, the carbon release was very rapid, $\delta^{18}O$

would substantially lag behind $\delta^{13}C$. The threshold can be determined as a function of the characteristic response time of the climate system and the specific nature of the isotope records and their associated uncertainty ('noise'), as detailed below. We emphasize that our approach is by no means restricted to the PETM onset but may be applied to other past climate perturbations, given high-resolution isotope records and a proper time scale of climate-carbon cycle changes.

Several possible candidate records with high sedimentation rates exist from the subsiding continental margin of the US east coast[16,20,21] (Fig. 1). However, currently only one section, from Millville, NJ, has cm-resolution bulk isotope records (foraminiferal isotopes at lower resolution)[22], potentially offering the highest fidelity recording of the onset[23,24] (Fig. 2). Although we use isotope records of bulk carbonate below that may have an unknown diagenetic overprint (see Supplementary Information), we argue that the relative sense and timing of change between $\delta^{13}C$ and $\delta^{18}O$ during the PETM onset has been retained. Indeed, both the $\sim$3‰ CIE across the onset and the concomitant $\sim$1‰ $\delta^{18}O$-drop at Millville (indicating $\sim$5 K warming) are consistent with most other pelagic sequences[9] and foraminifer isotope data from nearby sections at Bass River[20] and Wilson Lake[21,25] (Fig. 1). Most importantly, the Millville bulk isotope records are consistent with data from planktonic foraminifera at the same site[22], which lends confidence in our approach as foraminifera are considered robust recorders of changes in $\delta^{13}C$ and $\delta^{18}O$. For further discussion of the Millville records, including spectral analysis, bioturbation, couplets, and contamination, see Supplementary Information. We emphasize that the resolution of

other PETM sections across the onset (including at Bass River and Wilson Lake) is currently insufficient to determine leads and lags between δ^{13}C and δ^{18}O. We hence use the Millville record as the target for our approach and derive an estimate for the maximum rate of carbon release across the PETM onset.

First, we determine possible δ^{13}C-δ^{18}O leads/lags in the Millville records (depth-domain). Then we simulate carbon release (δ^{13}C) and climate response ($\simeq \delta^{18}$O) using carbon cycle/climate models, while varying the carbon release time. The fastest possible release that still yields leads/lags consistent with the data will provide the minimum time interval for the PETM onset.

Leads and lags

We determined potential leads/lags between the δ^{13}C and δ^{18}O Millville records for the non-stationary- and (transformed) stationary time series (Fig. 2). For the former, we focus on obvious leads/lags at the onset's start- and endpoint. The gap at $z = 0.41-0.46$ m (%$CaCO_3$<0.1%) prevents any lead/lag determination at the onset's endpoint. Zooming in on the start, δ^{13}C appears to lead δ^{18}O by one sample step in the depth-domain ($\Delta k = +1$, Fig. 2d, arrows). However, considering the immediate pre-onset variability, onset δ^{13}C and δ^{18}O values only exceed the minimum pre-onset values at three and one samples above the apparent onset, respectively, indicating a δ^{13}C-lag by one sample step ($\Delta k = -1$, Fig. 2d, circles). Five-point running mean curves (compared to maximum pre-onset values) would also indicate a slight δ^{13}C-lag relative to δ^{18}O. Altogether, we take $\Delta k = \pm 2$ as an estimated upper limit for possible

leads/lags between the non-stationary time series.

We also determined possible systematic leads/lags across the full records using time-series analysis. The raw data series ($X = \delta^{13}$C, $Y = \delta^{18}$O) are non-stationary and inadequate for determining leads/lags based on autocorrelation function (ACF) and cross-correlation function (CCF)[26,27]. Thus, we use first-order differencing:

$$x_i = X_{i+1} - X_i \; ; \qquad y_i = Y_{i+1} - Y_i \; . \tag{1}$$

The ACFs of the differenced series (Fig. 2) are similar to white-noise ACFs, except for significant negative correlations (95% level) at $\Delta k = \pm 1, \pm 2$, which can lead to spurious correlations in the CCF[26–28].

Indeed, CCF_{xy} shows a significant negative correlation at $\Delta k = +1$, which however disappears after prewhitening (series x', y', Supplementary Information). The single large peak in $\mathrm{CCF}_{x'y'}$ at $\Delta k = 0$ indicates a contemporaneous relationship. The correlation at $\Delta k = -6$ is barely significant and, in fact, 5 out of 100 (or 1/20) 'significant' correlations are expected at the 95% confidence level even if the series are truly random. Moreover, the correlation is *negative*, which is not relevant for a potential causal relationship between δ^{13}C and δ^{18}O (or *vice versa*) during carbon release and warming. Such a relationship requires a *positive* correlation, i.e. deviations towards lighter values in both records. Thus, within the limits of the data resolution (average Δz), we find a significant contemporaneous correlation ($\Delta k = 0$) but can not detect any significant leads/lags between the stationary series (full records). The same holds true for the stationary sub-series that only cover the onset or parts of

it (Supplementary Information). We conclude from the combined stationary and non-stationary analyses that $|\Delta k| \leq 2$ for possible leads/lags between the Millville δ^{13}C and δ^{18}O records.

Carbon cycle–climate modeling

The maximum lead/lag derived from the data records (τ_{dat}) provides a strong constraint for the carbon cycle/climate models in determining the minimum onset interval. Given a total carbon input and a model release time, the simulated lag (τ_{mod}) between surface temperature ($\simeq \delta^{18}$O) and δ^{13}C must not exceed τ_{dat} (time-domain) at lag = $max|\Delta k| \times \Delta z$ in the depth-domain:

$$\tau_{\mathrm{mod}} \leq \tau_{\mathrm{dat}} = max|\Delta k|\ \Delta z/\bar{r}_{\mathrm{sed}}\ , \qquad (2)$$

where $\Delta z = 0.234$ cm is the average sampling resolution across the onset and $max|\Delta k| = 2$ (see above). Furthermore, $\bar{r}_{\mathrm{sed}} = z_{\mathrm{in}}/t_{\mathrm{in}}$ (to be determined) represents an *average* sedimentation rate, where $z_{\mathrm{in}} = 24.8$ cm is the onset interval in the Millville core (Fig. 2a) and t_{in} is the model release time. Importantly, $r_{\mathrm{sed}}(t)$ does not need to be constant for our approach (see Supplementary Information). The final calculated $\bar{r}_{\mathrm{sed}} \simeq 6$ cm kyr^{-1} during the onset (see below) is consistent with foraminifer accumulation rates[24] and falls between rates within the basal PETM section at Bass River[21] (2.8 cm kyr^{-1}) and average PETM rates at Wilson Lake/Bass River[21] ($10 - 20$ cm kyr^{-1}).

Although τ_{dat} is not known a priori without a robust age model, we can

quantify τ_{mod} (and hence constrain the minimum value of τ_{dat}, Eq. (2)) using the carbon cycle/climate models GENIE[12] and LOSCAR[29,30] (Fig. 3). Note that lead-lag determination using cross-correlation is unsuitable for the model output. Model leads/lags were directly determined from the normalized response (see Supplementary Information). In addition to global mean sea-surface temperature (SST) and δ^{13}C, we analyzed GENIE's grid-point output on the North-West Atlantic shelf (NWA-shelf, corresponding to Millville's paleo-location, see Supplementary Information). For instance, at 3,000 Pg C (varied below) released over 2,000 yr, the SST response (ΔT) lags substantially behind model-δ^{13}C ($\tau_{\mathrm{mod}} \simeq 135$ yr, see Supplementary Information). In contrast, Eq. (2) gives τ_{dat} of only 38 yr at $t_{\mathrm{in}} = 2,000$ yr. At 3,000 Pg C input, GENIE's τ_{mod} on the NWA-shelf only approaches τ_{dat} for input times $\gtrsim 4,000$ yr (Figs. 3,4).

To evaluate the sensitivity of the calculated minimum onset interval to critical parameters, we varied the model release time, release pattern, total carbon input (2000, 3000, 4500 Pg C), climate sensitivity, initial (pre-event) $p\mathrm{CO}_2$ (Fig. 4), and atmospheric vs. deep-ocean carbon injection (Supplementary Information). (Note that for long release times, τ_{mod} reverses sign, i.e. SST starts leading δ^{13}C, see Supplementary Information.) Also, simulated δ^{13}C leads the model climate response at the onset's start because the models are forced by carbon input. In reality, temperature may have led carbon input initially[5,31], although the data do not support any significant δ^{18}O-lead at the start (Fig. 2d). Nevertheless, we consider this potential bias when determining model time lags (Supplementary Information).

GENIE's NWA-shelf response indeed represents the shortest τ_{mod} of all scenarios tested. The intercept of the shortest τ_{mod} and τ_{dat} yields the minimum onset interval consistent with the data, namely ~4,000 yr (Fig. 4).

Data uncertainties and implications

Our analysis yields an average sedimentation rate of 6.2 cm kyr^{-1} at $t_{\mathrm{in}} = 4,000$ y and thus an average sampling resolution of ~40 years at Millville. Hence we cannot rule out brief pulses of carbon input above average rates on time scales $\lesssim$ 40 yr (a similar limitation arises from time-averaging of the primary signal in sediments). However, if such pulses occurred, their contribution to the maximum sustained rate must have been small. Otherwise, δ^{13}C would show large, rapid step-like drops following such pulses, which is not the case (Fig. 2a). Our results do not support a 2-step carbon release[32] for which the effect of bioturbation and mixing with our estimated sedimentation rate at Millville would only damp, not obliterate, a prominent δ^{13}C reversal midway through the onset. We note that a previous study determined leads/lags between climatic/biotic events at one PETM site[33]. However, the data and model results were not used to constrain the time interval of the onset. Most importantly, the simulation assumed instantaneous carbon release – unsuitable for our approach.

We also consider that the end of the onset interval at Millville could be located within the gap at $z = 0.41-0.46$ m (%$CaCO_3$<0.1%, Fig. 2). If the onset-end occurred at 0.46 m (20% larger z_{in} for a given t_{in}), the average sedimentation rate would be

higher and τ_{dat} smaller (Eq. (2)). For a smaller τ_{dat}, the intercept with τ_{mod} occurs later (Fig. 4), which would give a *longer* duration for the calculated onset interval. While it is unlikely that z_{in} was initially smaller and subsequently smoothed/expanded by say bioturbation (Supplementary Information), we also illustrate the effect of a 20% smaller z_{in} on τ_{dat} (Fig. 4).

The initial carbon release during the PETM onset thus occurred over at least 4,000 yr. Using estimates of 2,500-4,500 Pg C for the initial carbon release, the maximum sustained PETM carbon release rate was therefore 0.6-1.1 Pg C yr^{-1}. Given currently available paleorecords, we conclude that the present anthropogenic carbon release rate ($\sim$10 Pg C yr^{-1}) is unprecedented during the Cenozoic (past 66 Myr). Possible known consequences of the rapid man-made carbon emissions have been extensively discussed elsewhere[2,30,34,35]. Regarding impacts on ecosystems, the present/future rate of climate change and ocean acidification[12,36,37] is too fast for many species to adapt[38], likely resulting in widespread future extinctions in marine and terrestrial environments that will substantially exceed those at the PETM[13]. Given that the current rate of carbon release is unprecedented throughout the Cenozoic, we have effectively entered an era of no-analogue state, which represents a fundamental challenge to constraining future climate projections.

Code availability. The C code for the LOSCAR model can be obtained from the author (R.E.Z.) upon request (loscar.model@gmail.com).

Author Contributions. R.E.Z. led the effort. All authors wrote the paper.

The authors declare no competing financial interests.

Correspondence and requests for materials should be addressed to R.E.Z.

Acknowledgments. We thank two anonymous reviewers for comments that improved the manuscript. We also thank Ellen Thomas for sharing data and Gabe Bowen for discussions. This research was supported by NSF grant OCE12-20602 to J.C.Z. and R.E.Z. and EU grant ERC-2013-CoG-617313 to A.R.

References

1. Le Quéré et al. Global carbon budget 2015. *Earth Syst. Sci. Data*, 7(2):349–396, (2015).

2. IPCC, Intergovernmental Panel on Climate Change, Stocker, T. F. et al. (Eds.). *Climate Change 2013: The Physical Science Basis*. Cambridge University Press, Cambridge, pp. 1535, (2013).

3. Zachos, J. C., Dickens, G. R., & Zeebe, R. E. An early Cenozoic perspective on greenhouse warming and carbon-cycle dynamics. *Nature*, 451:279–283, doi:10.1038/nature06588, (2008).

4. Rohling, E. J. et al. Making sense of palaeoclimate sensitivity. *Nature*, 491:683–691, doi:10.1038/nature11574, (2012).

5. Dickens, G. R., O'Neil, J. R., Rea, D. K., & Owen, R. M. Dissociation of oceanic methane hydrate as a cause of the carbon isotope excursion at the end of the Paleocene. *Paleoceanogr.*, 10:965–971, (1995).

6. Zachos, J. C., Pagani, M., Sloan, L., Thomas, E., & Billups, K. Trends, rhythms, and aberrations in global climate 65 Ma to present. *Science*, 292:686–693, (2001).

7. Zachos, J. C., Röhl, U., Schellenberg, S. A., Sluijs, A., Hodell, D. A., Kelly, D. C., Thomas, E., Nicolo, M., Raffi, I., Lourens, L. J., McCarren, H., & Kroon, D. Rapid acidification of the ocean during the Paleocene-Eocene Thermal Maximum. *Science*, 308:1611–1615, (2005).

8. Zeebe, R. E., Zachos, J. C., & Dickens, G. R. Carbon dioxide forcing alone insufficient to explain Palaeocene-Eocene Thermal Maximum warming. *Nature Geosci.*, 2:576–580, doi:10.1038/ngeo578, (2009).

9. McInerney, F. A. & Wing, S. L. The Paleocene-Eocene Thermal Maximum: A Perturbation of Carbon Cycle, Climate, and Biosphere with Implications for the Future. *Ann. Rev. Earth Planet. Sci.*, 39(1):489–516, (2011).

10. Rogner, H. An assessment of world hydrocarbon resources. *Ann. Rev. Energy Environ.*, 22: 217–262, (1997).

11. McGlade, C. & Ekins, P. The geographical distribution of fossil fuels unused when limiting global warming to 2°C. *Nature*, 517:187–190, (2015).

12. Ridgwell, A. & Schmidt, D. Past constraints on the vulnerability of marine calcifiers to massive carbon dioxide release. *Nature Geosci.*, 3:196–200, doi:10.1038/ngeo755, (2010).

13. Zeebe, R. E. & Zachos, J. C. Long-term legacy of massive carbon input to the Earth system: Anthropocene vs. Eocene. *Royal Soc. London Phil. Trans. A*, 29, (2013).

14. Farley, K. A. & Eltgroth, S. F. An alternative age model for the Paleocene-Eocene thermal maximum using extraterrestrial ^{3}He. *Earth Planet Sci. Lett.*, 208:135–148, (2003).

15. Murphy, B. H., Farley, K. A., & Zachos, J. C. An extraterrestrial ^{3}He-based timescale for the Paleocene-Eocene thermal maximum (PETM) from Walvis Ridge, IODP Site 1266. *Geochim. Cosmochim. Acta*, 74:5098–5108, (2010).

16. John, C. M., Bohaty, S. M., Zachos, J. C., Sluijs, A., Gibbs, S., Brinkhuis, H., & Bralower, T. J. North American continental margin records of the Paleocene-Eocene thermal maximum: Implications for global carbon and hydrological cycling. *Paleoceanogr.*, 23:PA2217, doi:10.1029/2007PA001465, (2008).

17. Hansen, J. and Russell, G. and Lacis, A. and Fung, I. and Rind, D. and Stone, P. Climate Response Times: Dependence on Climate Sensitivity and Ocean Mixing. *Science*, 229: 857–859, (1985).

18. Roe, G. Feedbacks, Timescales, and Seeing Red. *Ann. Rev. Earth Planet. Sci.*, 37:93–115, (2009).

19. Hansen, J., Sato, M., Kharecha, P., & von Schuckmann, K. Earth's energy imbalance and implications. *Atmos. Chem. Phys.*, 11:13421–13449, (2011).

20. Zachos, J. C., Bohaty, S. M., John, C. M., McCarren, H., Kelly, D. C., & Nielsen, T. The Paleocene-Eocene carbon isotope excursion: Constraints from individual shell planktonic foraminifer records. *Royal Society Phil. Trans. A*, 365:1829–1842, doi:10.1098/rsta.2007.2045, (2007).

21. Stassen, P., Thomas, E., & Speijer, R. P. Integrated stratigraphy of the Paleocene-Eocene thermal maximum in the New Jersey Coastal Plain: Toward understanding the effects of global warming in a shelf environment. *Paleoceanogr.*, 27:PA4210, (2012).

22. Makarova, M., Miller, K. G., Wright, J. D., Rosenthal, Y., & Babila, T. Temperature and salinity changes associated with the Paleocene-Eocene Carbon Isotope Excursion along the mid Atlantic margin. *AGU Fall Meeting*, :Abstract PP33C–2322, (2015).

23. Wright, J. D. & Schaller, M. F. Evidence for a rapid release of carbon at the Paleocene-Eocene thermal maximum. *Proc. Nat. Acad. Sci.*, 110:15,908–15,913, (2013).

24. Pearson, P. N. & Thomas, E. Drilling disturbance and constraints on the onset of the Paleocene-Eocene boundary carbon isotope excursion in New Jersey. *Clim. Past*, 11: 95–104, (2015).

25. Zachos, J. C., Schouten, S., Bohaty, S., Sluijs, A., Brinkhuis, H., Gibbs, S., Bralower, T., & Quattlebaum, T. Extreme warming of mid-latitude coastal ocean during the Paleocene-Eocene Thermal Maximum: Inferences from TEX_{86} and isotope data. *Geology*, 34:737–740, (2006).

26. Wei, W. W. S. *Time Series Analysis: Inivariate and Multivariate Methods*. Addison-Wesley, pp. 478, (1990).

27. Chatfield, C. *The Analysis of Time Series: An Introduction*. CRC Press, pp. 333, 6th edition, (2004).

28. Box, G. E. P. & Jenkins, G. M. *Time Series Analysis: Forecasting and Control*. Holden-Day, San Franciso, CA, (1970).

29. Zeebe, R. E. LOSCAR: Long-term Ocean-atmosphere-Sediment CArbon cycle Reservoir Model v2.0.4. *Geosci. Model Dev.*, 5:149–166, (2012).

30. Zeebe, R. E. Time-dependent climate sensitivity and the legacy of anthropogenic greenhouse gas emissions. *Proc. Nat. Acad. Sci.*, 110:13739–13744, (2013).

31. Sluijs, A., Brinkhuis, H., Schouten, S., Bohaty, S., John, C., Zachos, J. C., Reichart, G. J., Sinninghe Damste, J. S., Crouch, E. M., & Dickens, G. R. Environmental precursors to rapid light carbon injection at the Palaeocene/Eocene boundary. *Nature*, 450:1218–1221, (2007).

32. Bowen, G. J., Maibauer, B. J., Kraus, M. J., Röhl, U., Westerhold, T., Steimke, A., Gingerich, P. D., Wing, S. L., & Clyde, W. C. Two massive, rapid releases of carbon during the onset of the Palaeocene-Eocene Thermal Maximum. *Nature Geosci.*, 8:44–47, (2015).

33. Bralower, T. J., Meissner, K. J., Alexander, K., & Thomas, D. J. The dynamics of global change at the Paleocene-Eocene thermal maximum: A data-model comparison. *Geochemistry, Geophysics, Geosystems*, 15:3830–3848, (2014).

34. National Research Council. *Abrupt Impacts of Climate Change: Anticipating Surprises*. The National Academies Press, Washington, DC, pp. 250, (2013).

35. Robinson, A., Calov, R., & Ganopolski, A. Multistability and critical thresholds of the Greenland ice sheet. *Nature Clim. Change*, 2:429–432, (2012).

36. Caldeira, K. & Wickett, M. E. Anthropogenic carbon and ocean pH. *Nature*, 425:365, (2003).

37. Zeebe, R. E., Zachos, J. C., Caldeira, K., & Tyrrell, T. Oceans: Carbon Emissions and Acidification (in Perspectives). *Science*, 321:51–52, doi:10.1126/science.1159124, (2008).

38. Rockström, J. et al. A safe operating space for humanity. *Nature*, 461:472–475, (2009).

Figure 1. Selected stable isotope records from NJ margin sections across the PETM onset[16,20,21,23]. (a) Carbon (δ^{13}C) and (b) oxygen (δ^{18}O) isotopes plotted vs. position in core (the $z = 0$ m alignment is arbitrary). Also, in the depth-domain, the length of the onset interval cannot be compared between locations because of different sedimentation rates. Subb. = species of *Subbotina* (planktonic foraminifer). Open (filled) diamonds indicate all (mean) Subb. values. Note that the Millville bulk isotope records are consistent with data from planktonic foraminifera at the same site[22].

Figure 2. Millville PETM records and time-series analysis. (a) Bulk stable carbon and oxygen isotopes ($X = \delta^{13}$C, $Y = \delta^{18}$O). Time runs to the right (oldest sample was assigned depth $z = 0$ m). (b) First-order differenced time series (x, y) and prewhitened (filtered) series (x', y'), see text. (c) Leads/lags based on autocorrelation function (ACF) and cross-correlation function (CCF). Dashed horizontal lines: 95% confidence interval ($\sim \pm 2/\sqrt{N} \simeq 0.12$). After prewhitening, $\mathrm{CCF}_{x'y'}$ (gray squares) only shows significant correlation at $\Delta k = 0$ (contemporaneous) and at $\Delta k = -6$ (see text). (d) Leads/lags between Millville δ^{13}C (red) and δ^{18}O (blue) at the start of the PETM onset. Arrows: apparent start based on superficial visual inspection. Gray bars: range of pre-onset variability. Circles: first onset samples exceeding pre-onset variability. Dashed lines: 5-point running means.

Figure 3. Examples of model time lags (τ_{mod}) as a function of model release time (t_{in}). $\tau_{dat} = 2\Delta z/\bar{r}_{sed}$ indicates the maximum lead/lag allowed by the time-series analysis of the data records (see text). Note different time axes. All records and model output are normalized to %response. Simulated δ^{13}C leads the model climate response at the onset's start because the models are forced by carbon input. In reality, temperature may have led carbon input initially[5,31], although the data do not support any significant δ^{18}O-lead at the start (Fig. 2d). Nevertheless, to avoid potential model bias during the initial onset phase, we determine τ_{mod} as an average model lag, omitting the initial 40% of the normalized response (see Supplementary Information). Scenario (a) is not feasible as τ_{mod} substantially exceeds τ_{dat}. Note that τ_{dat} is not to be determined from the raw (non-stationary) data records but from the first-order differenced and prewhitened time series using cross-correlation (see text and Supplementary Information).

Figure 4. Determining the minimum release time. Maximum lead/lag is based on data records (τ_{dat}) and model time lag (τ_{mod}) calculated using carbon cycle/climate models GENIE[12] and LOSCAR[29,30], see text. The intercept of the shortest τ_{mod} and τ_{dat} yields the minimum onset interval consistent with the data ($\sim$4,000 yr, arrow). The dashed purple lines illustrate potential uncertainties in τ_{dat} from variations in the onset length in the Millville core ($z_{in}\pm$20%, though see text and Supplementary Information). Standard model runs use 3000 Pg C carbon input and climate sensitivity $S_{2\times} = 3$ K per CO_2 doubling. Sensitivity of τ_{mod} was tested by varying the model release time (horizontal axis), total carbon input (open symbols: 2000, 3000, and 4500 Pg C), carbon release patterns (Rate: Up, Down, Noise), climate sensitivity ($S_{2\times}$), initial (pre-event) pCO_2 (750$-$1000 ppmv), and atmospheric vs. deep-ocean carbon injection (see Supplementary Information). NW Atl shelf = GENIE grid-point output on the North-West Atlantic shelf corresponding to Millville's paleo-location (see Supplementary Information).

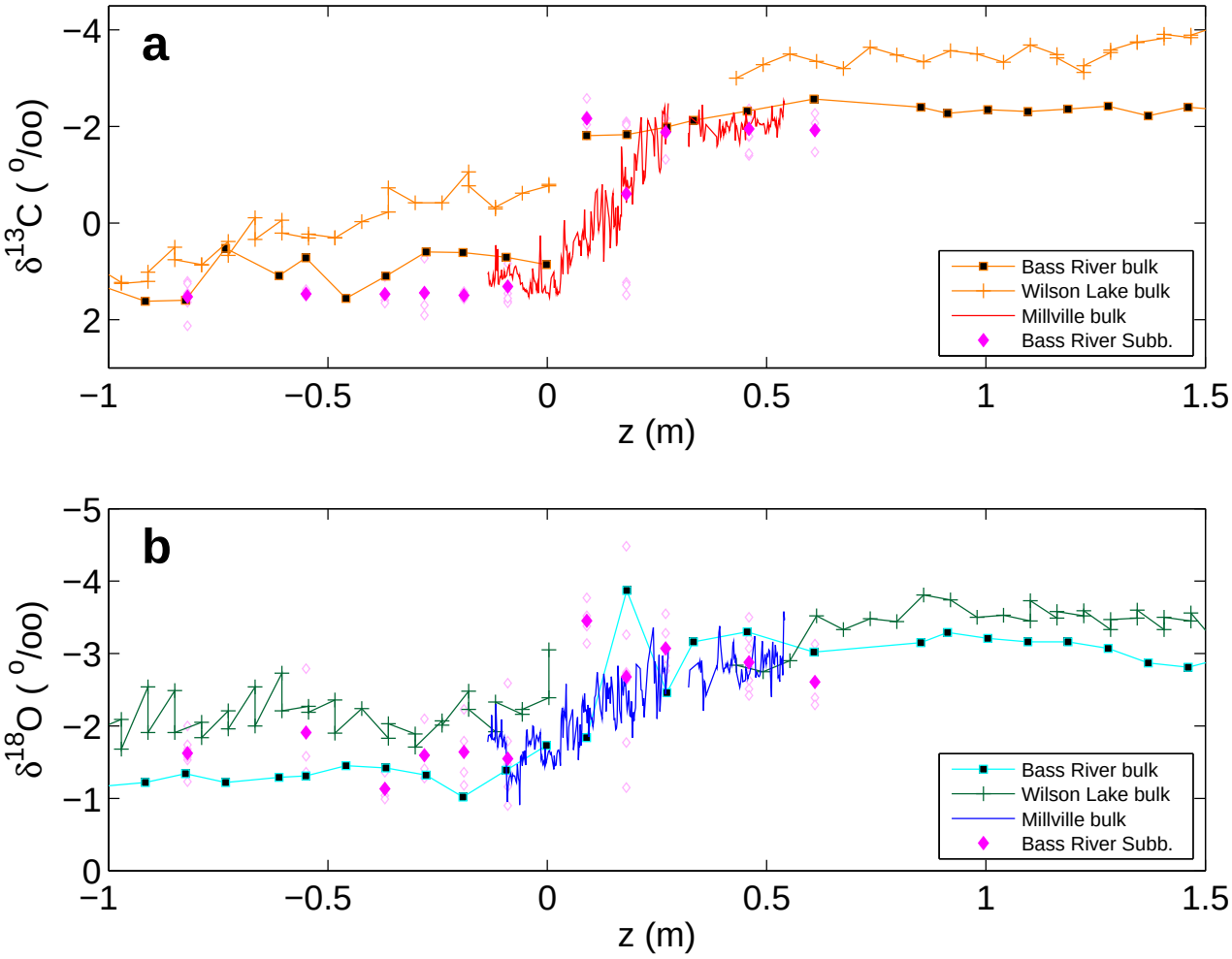
a
b
$\delta^{13}C$ ($^{o}/_{oo}$)
$\delta^{18}O$ ($^{o}/_{oo}$)
z (m)
Bass River bulk
Wilson Lake bulk
Millville bulk
Bass River Subb.

Figure 1.

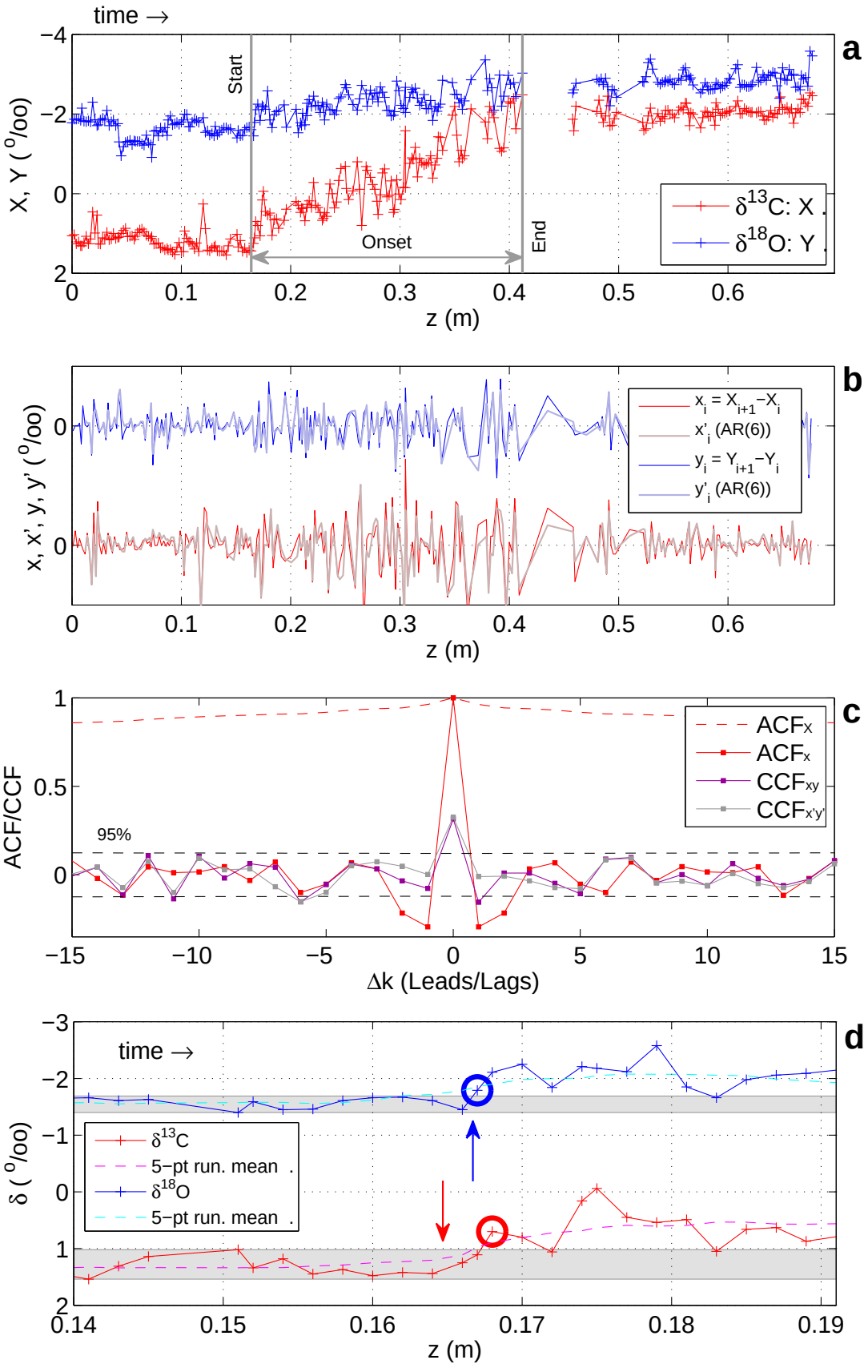
time →
a
Start
Onset
End
X, Y (°/oo)
z (m)
δ13C: X
δ18O: Y
b
x, x', y, y' (°/oo)
xi = Xi+1−Xi
x'i (AR(6))
yi = Yi+1−Yi
y'i (AR(6))
c
ACF/CCF
95%
ACFX
ACFx
CCFxy
CCFx'y'
Δk (Leads/Lags)
d
time →
δ (°/oo)
δ13C
5−pt run. mean
δ18O
5−pt run. mean

Figure 2.

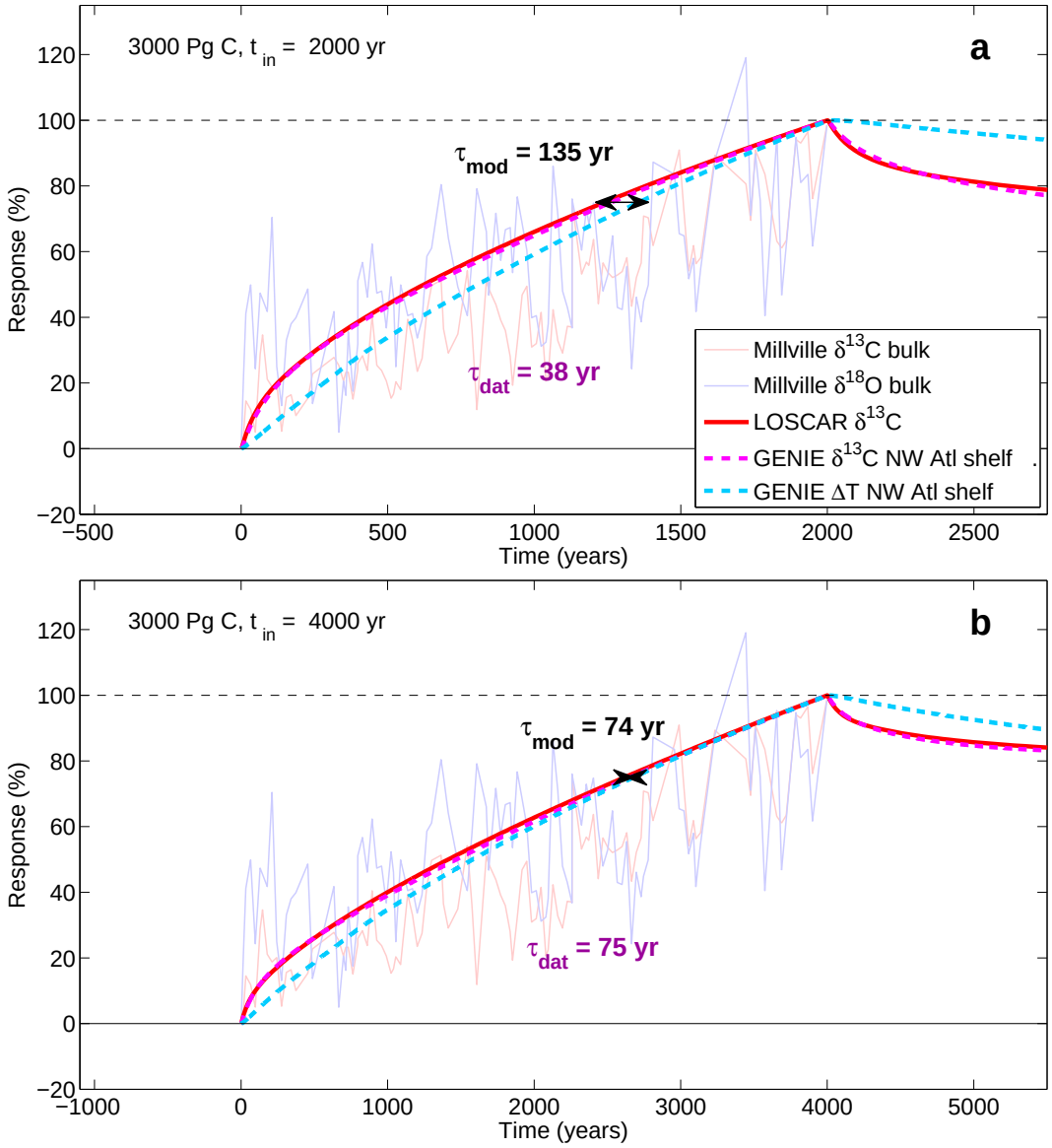
3000 Pg C, t in = 2000 yr
a
τmod = 135 yr
τdat = 38 yr
Millville δ13C bulk
Millville δ18O bulk
LOSCAR δ13C
GENIE δ13C NW Atl shelf
GENIE ΔT NW Atl shelf
Response (%)
Time (years)
3000 Pg C, t in = 4000 yr
b
τmod = 74 yr
τdat = 75 yr
Response (%)
Time (years)

Figure 3.

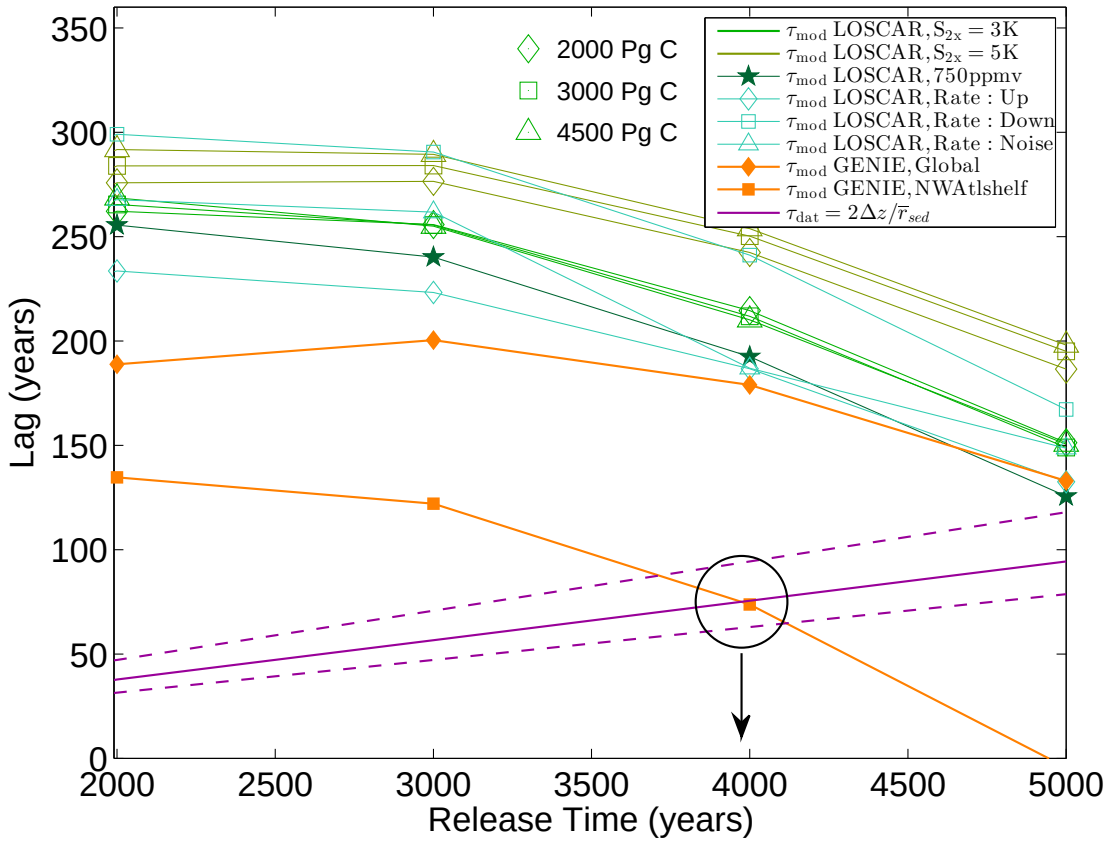
2000 Pg C
3000 Pg C
4500 Pg C
τ_{mod} LOSCAR, $S_{2x} = 3K$
τ_{mod} LOSCAR, $S_{2x} = 5K$
τ_{mod} LOSCAR, 750ppmv
τ_{mod} LOSCAR, Rate : Up
τ_{mod} LOSCAR, Rate : Down
τ_{mod} LOSCAR, Rate : Noise
τ_{mod} GENIE, Global
τ_{mod} GENIE, NWAtlshelf
$\tau_{\mathrm{dat}} = 2\Delta z / \overline{r}_{sed}$
Lag (years)
Release Time (years)
0
50
100
150
200
250
300
350
2000
2500
3000
3500
4000
4500
5000

Figure 4.